Thermophysical Properties of Graphene Nanosheets – Hydrogenated Oil Based Nanofluid for Drilling Fluid Improvements

Accepted Manuscript

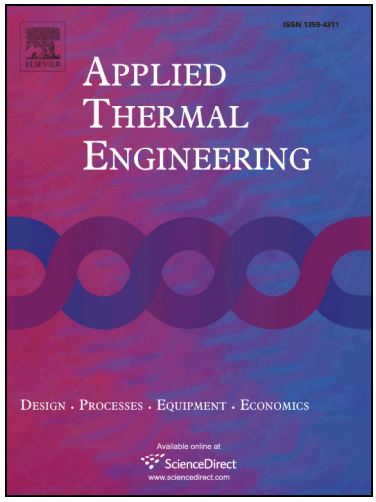

Thermophysical Properties of Graphene Nanosheets – Hydrogenated Oil Based Nanofluid for Drilling Fluid Improvements

Yee Ho Chai, Suzana Yusup, Vui Soon Chok, Sonny Irawan, Jespal Singh Deol Balbir Singh

PII: S1359-4311(17)30352-6
DOI: http://dx.doi.org/10.1016/j.applthermaleng.2017.05.012
Reference: ATE 10323

To appear in: *Applied Thermal Engineering*

Received Date: 17 January 2017
Revised Date: 29 March 2017
Accepted Date: 4 May 2017

Please cite this article as: Y. Ho Chai, S. Yusup, V. Soon Chok, S. Irawan, J. Singh Deol Balbir Singh, Thermophysical Properties of Graphene Nanosheets – Hydrogenated Oil Based Nanofluid for Drilling Fluid Improvements, *Applied Thermal Engineering* (2017), doi: http://dx.doi.org/10.1016/j.applthermaleng.2017.05.012

Thermophysical Properties of Graphene Nanosheets – Hydrogenated Oil Based Nanofluid for Drilling Fluid Improvements

Yee Ho Chai[a], Suzana Yusup[a*], Vui Soon Chok[b], Sonny Irawan[c], Jespal Singh Deol Balbir Singh[d]

[a]Biomass Processing Lab, Center for Biofuel and Biochemical, Green Technology, Mission Oriented Research, Chemical Engineering Department, Universiti Teknologi PETRONAS, Bandar Seri Iskandar, 31750, Tronoh, Perak, Malaysia

[b]Chemical Engineering Department, Heriot-Watt University Malaysia, No. 1, Jalan Venna P5/2, Precinct 5, 62200 Putrajaya, Malaysia

[c]Petroleum Engineering Department, Universiti Teknologi PETRONAS, Bandar Seri Iskandar, 31750, Tronoh, Perak, Malaysia

[d]Graphene Nanochem Plc, Suite 0.2, Level 9, WORK@Clearwater Changkat Semantan, Off Jalan Semantan, Damansara Heights, 50490, Kuala Lumpur, Malaysia

Corresponding author. Tel: +60 53687642, Fax: +60 53688204

Email address: yeeho.chai@gmail.com (Y.H. Chai),
drsuzana_yusuf@utp.edu.my ; drsuzana_yusuf@petronas.com.my (S. Yusup),
V.Chok@hw.ac.uk (V.S. Chok),
drsonny_irawan@utp.edu.my (S. Irawan)
jespal@platinumgroup.com.my (J.Singh)

ABSTRACT

In this study, thermophysical properties of graphene nanosheets – hydrogenated oil based nanofluid was investigated for the improvement of drilling fluids. Graphene nanosheets powder were dispersed through two-steps method which utilizes hydrodynamic and acoustic cavitation (HAC) combination process. The weight concentrations of dispersed graphene nanosheets powder in this study are 25 ppm, 50 ppm and 100 ppm respectively. The thermophysical properties investigated include thermal conductivity and rheological properties of graphene nanosheet – hydrogenated oil based nanofluid. At the highest nanoparticle concentration, thermal conductivity (TC) enhancement is able to reach up to 14.4% at 50°C while viscosity and shear stress values increased up to 33% at 30°C. Both

properties are observed to increase with respect to nanoparticle concentrations. The TC models were able to predict consistently with experimental data at lower nanoparticle concentration but underpredicted at higher nanoparticle concentration. The Bingham model has proven to fit well with the rheological data obtained in this study. Cavitation number, K and coefficient of discharge, C_D parameters used to evaluate hydrodynamic cavitation dispersion were found to be 1.025 and 0.3313 respectively. Both parameters had denoted that hydrodynamic cavitation had taken place in the system successfully.

Keywords: Graphene nanosheets; Hydrogenated oil; Thermal conductivity; Rheological behaviour; Hydrodynamic cavitation

Nomenclatures:

μ	dynamic viscosity of liquid
μ_{max}	maximum velocity
C_D	coefficient of discharge
$d_{orifice}$	orifice diameter
K	cavitation number
k_{bf}	thermal conductivity of base fluid
k_{eff}	effective thermal conductivity of nanoparticle
k_{nf}	thermal conductivity of nanofluid
k_p	thermal conductivity of nanoparticle
M	mass flow rate
n	shape factor of nanoparticle
p_{in}	inlet pressure
p_{vap}	vapour pressure of liquid
Re	Reynold's number
γ	shear rate
Δp	inlet and outlet pressure difference
ρ_l	density of liquid
σ	shear stress
σ_o	limiting shear stress

φ volume fraction of nanoparticle

1. Introduction

It is reported that more than 50% of the current world reserves are 4,200 m below sea level with temperature and pressure exceeding 200°C and 1600 bar respectively [1]. The stability of drilling fluids deteriorates when subjected to high temperature and high pressure (HTHP) applications. Drilling fluids subjected to HTHP applications often result in wear and tear of drilling tools and equipment [2]. Several main limitations include costly materials and treatment costs, increase in fluid density and inability to perform under HTHP conditions [3]. Singh and Ahmed [4] explained that the increased in surface interactions between particles allow heat to be conducted more efficiently. Not only that, the disposal of waste oil-based mud to the surroundings resulted in pollution of the oceans and killing off the coral reefs [3]. The need for a biodegradable and environmental friendly drilling fluid is inevitable to preserve the marine environment. The search of a base fluid that could biodegrade anaerobically led to the discovery of esters which would biodegrade with the presence of "built-in" oxygen present in the esters [5]. The challenges of vegetable oil or esters as drilling fluids are reported to have high viscosity properties and rapid deterioration at high temperature [6]. The application of graphene nanosheets as nanomaterials to improve the thermophysical properties of a biodegradable drilling fluid is proposed to overcome the limitations.

Nanofluids are a relatively new class of fluids which consist of base fluids having metallic or non-metallic nanoparticle suspensions with average sizes of 100 nm or less [7] that consist of condensed nanoparticles that act as a colloidal suspensions. Since the first synthesised carbon nanotube nanofluid by Stephen U.S. Choi in 1995, there has been an escalating number nanofluidics-related publications and its applications. Numerous

nanofluids applications have revolutionised various industries globally including industrial with heat transfer applications [8], electronic cooling systems [9], cooling and lubrication of drilling fluids [10] and etc as nanofluids possess anomalous physical properties compared to its base fluids counter-part.

Graphite contains multiple layers of planar structures where each layers are termed graphene. First discovered by Novoselove et al. [11], the arrangement is usually honeycomb lattice structure with interplanar distance between each layer of graphene at approximately 0.335 nm and atomic separation of 0.142 nm. The thickness between each sheets are roughly distanced at 0.34 nm. Graphene has been reportedly to have high carrier mobility, high Young's modulus strength and high intrinsic thermal conductivity. The intrinsic value of thermal conductivity of a freely suspended single layer graphene at room temperature is valued between 2000 – 4000 W/m.K [12]. Some has even reported up to as high as 5300 W/m.K [13]. As graphene is a two – dimensional material, the heat transfer properties of graphene will be significantly different as compared to zero dimensional and one dimensional nanoparticles [14]. This anomalous heat transfer conductance enables graphene to be a potential source for the improvement of existing coolants.

Ahammed et al. [15] had carried out thermal conductivity comparisons between graphene against other metal oxide nanoparticles. They discovered that at very low volume concentration of 0.15 vol%, is are able to thermal conductivity enhancement by 37.2% at 50°C with graphene-water. When compared to silver-water at similar temperature, graphene supersedes by 5.2%. Yu et al. [16] compared 5.0 vol% of graphene-ethylene glycol nanofluid against graphene oxide and discovered graphene to possess higher thermal conductivity enhancement by 42%. They deduced this to the presence of oxygen atoms and saturated sp^3 bonds which limited the thermal conductance across graphene oxide. Ma et al. [17] had

investigated the effect of functionalized graphene nanosheets into silicon oil at 0.07 wt% up to 60°C. The maximum thermal conductance enhancement achieved in their study was 18.9%.

However, the rheological aspect of the drilling fluids should also be considered. High viscosity properties of drilling fluids allows solid cuttings to be suspended whilst preventing sagging simultaneously [18] as excessive inclusion of nanoparticle concentrations prove to be disadvantageous. Vajjha and Das [19] discovered that the maximum theoretical particle loading allowable in a solution is 3 vol% where particle loadings greater than that will incur greater pressure drop and higher pumping operation cost.

In this study, graphene nanosheets was dispersed into hydrogenated oil – based drilling fluid via two – steps method which utilized hydrodynamic cavitation as the dispersion process. The thermophysical properties investigated in this study are thermal conductivity and rheological behaviour properties of graphene nanosheets – hydrogenated oil based nanofluids.

2. Experimental procedure

2.1 Materials

Hydrogenated oil-based drilling fluid and graphene nanosheets were procured from Platinum Green Chemicals Sdn. Bhd., Malaysia where the materials were used as received. Table 1 outlined the physical properties of the materials used in this study.

INSERT TABLE 1 HERE

2.2 Nanofluid preparation

The dispersion of graphene nanosheets was carried out using a two – steps method that utilized hydrodynamic cavitation dispersion to implode bubbles and break down agglomerates into smaller sizes. In this study, the dispersion of graphene nanosheets was

carried out in three steps, mainly pre-homogenization, hydrodynamic cavitation homogenization and post-homogenization. The investigating weight concentrations of graphene nanosheets are 25 ppm, 50 ppm and 100 ppm respectively.

Pre – homogenization was carried out with a high speed stirrer (VELP Scientifica Digital Overhead Stirrer – DLS) at 800 rpm for 15 minutes to homogenize graphene nanosheet powder into hydrogenated oil before being transferred to hydrodynamic cavitation system. The hydrodynamic cavitation dispersion process of graphene nanosheets was described similarly to our previous work [20].

INSERT FIG. 1 HERE

Post-homogenization involved transferring of hydrodynamic cavitated samples to bath ultrasonicator (Bath Ultrasonic Branson 8510E – DTH) to prevent aggregation of nanoparticles. The time duration taken for ultrasonication is 3 hours. The power and frequency of the bath ultrasonicator is 320 W and 40 kHz respectively. Fig. 2 shows the readily dispersed graphene nanosheets – hydrogenated oil nanofluid.

INSERT FIG. 2 HERE

2.3 Thermal conductivity analysis

KD2 Pro Thermal Properties Analyzer is selected to carry out thermal conductivity analysis of graphene nanosheet – hydrogenated oil nanofluid in this study as it uses transient heat line source method for thermal conductivity detection. The KD2 Pro is equipped with a sensor (1.3 mm diameter x 60 mm length). The thermal conductivity range for this sensor is between 0.02 W m^{-1} K^{-1} to 2.00 W m^{-1} K^{-1} with 0.001°C sensitivity.

KD2 Pro Thermal Properties Analyzer was pre-calibrated before each analysis with glycerol at room temperature to ensure the accuracy of the sensor. The glycerol sample was left to equilibrate for 15 minutes before taking calibration readings to ensure no free convection occurs within the sample.

Graphene nanosheet-hydrogenated oil nanofluids were sonicated before each thermal conductivity analysis to ensure homogeneity of the samples. The sonicated samples were left to equilibrate in water bath (Memmert Water Bath) for 20 minutes to ensure temperature equilibrium between samples and external temperature to eliminate free and forced convection of the samples.

In this analysis, there are two parametric studies which are the study of the effects of temperature and the effects of nanoparticle concentrations on thermal conductivity properties of hydrogenated oil nanofluid. The temperature parameter ranged from 30°C to 50°C with an increment of 5°C at each interval step. Thermal conductivity analysis of each graphene nanosheets concentrations were repeated four times for each temperature set.

2.3 Rheological behaviour analysis

The effects of temperature and nanoparticle concentrations on the viscosity and shear stress of hydrogenated oil-based nanofluid were also investigated. Malvern Bohlin Gemini II Rheometer were used to measure rheological properties of hydrogenated oil-based nanofluid.

The variation of temperature was controlled by a PC controlled Peltier plate controller. Selection of spindle used in this study consisted of cone-and-plate stainless spindle with 2^{o} angle and 40 mm diameter. The gap distance between spindle and Peltier plate was set constant at 30 μm to avoid jamming of particulates at the cone truncation. All data measurements and collections carried out consist of a delay time and integration time of 10 seconds to ensure steady-state conditions with estimated 3% deviation in measurement.

Samples were subjected to discontinuous shearing at shear rate ranging from 0 – 140 s^{-1} with 20 s^{-1} increment step at each temperature of 30°C, 40°C and 50°C respectively. Each runs were repeated 3 times to avoid measurement of deformed samples due to shearing process.

2.4 Evaluation of hydrodynamic cavitation

For the evaluation of hydrodynamic cavitation for the production of graphene nanosheets-hydrogenated oil-based nanofluids, several parameters namely Reynold's number (*Re*), coefficient of discharge (C_D) and cavitation number (*K*), were calculated.

In order to determine the value of *K*, the maximum velocity (μ_{max}) at orifice was calculated using Eq. 1 [21].

$$\mu_{\max} = \frac{M}{\Pi\left(\frac{d_{orifice}^2}{2}\right)\rho_l} \tag{1}$$

where $d_{orifice}$ is the orifice diameter, ρ_l is the liquid density and *M* is the mass flow rate.. The calculation of cavitation number (*K*) as shown in Eq. 2 [22] requires the inlet pressure at the orifice and the vapour pressure of the liquid to be known. As the cavitation process is carried out at open ends, the inlet pressure was taken to be atmospheric pressure while the vapour pressure was taken to be 100 Pa according to the specification sheet provided by the supplier. The calculation of *K* value is as follows:

$$K = \frac{2\left(p_{in} - p_{vap}\right)}{\rho_l . u_{\max}^2} \tag{2}$$

where p_{in} is the inlet pressure and p_{vap} is the vapour pressure of liquid.

Coefficient of discharge (C_D) was also used to evaluate the effectiveness of

hydrodynamic cavitation process. The calculation of C_D was given by Eq. 3 [21].

$$C_D = \frac{\rho_l . \mu_{\max}}{\sqrt{2.\rho_l . \Delta p}} \tag{3}$$

where Δp is the pressure difference between inlet pressure and outlet pressure at the orifice. Furthermore, Reynold's number (*Re*) is considered to further validate hydrodynamic cavitation process where $\sqrt{Re} > 60$ is considered to be a fully developed turbulent flow for a single stage high pressure homogenizer [21]. The calculation of *Re* is as shown in Eq. 4 [21].

$$\sqrt{\mathrm{Re}} = \sqrt{\frac{\rho_l u_{\max} d_{orifice}}{\mu}} \tag{4}$$

where μ is the dynamic viscosity of hydrogenated oil.

The diameter of the orifice used in this study is a one-hole orifice with outer diameter of 0.001 m connected to a 1/2 inch stainless steel pipe (SS304). Table 2 shows a summary of the key parameters considered in this study.

INSERT TABLE 2 HERE

3. Results and discussions

3.1 Graphene nanosheets analysis

The size and morphology of graphene nanosheets were taken using transmission electron microscopy (TEM, LIBRA Microscope 200) at magnification range of 20,000x and 800,000x as shown in Fig. 3(a) and Fig.3(b) respectively. From Fig. 3(a), the image depicted contrasting colours with few layers of graphene nanosheets stacked on each other. On that note, Fig. 3(b) showed a flat smooth surface with multi-walled graphene sheets at the boundary of graphene nanosheet stacks.

INSERT FIG. 3(a) AND FIG. 3(b) HERE

Fourier Transform Infrared (FTIR) spectra of graphene nanosheets is as shown in Fig. 4. Within the range between 2800 – 3500 cm^{-1}, a broad and sharp peak is found denoting the presence of –OH groups. This is in good agreement with the presence of stretching vibrations of –OH bonds [23]. The presence of alkynes is also represented by a weak peak at the range of 2200 – 3000 cm^{-1} which denoted little or no changes in dipole moment. At 1411 cm^{-1}, a C-C in-ring aromatics exhibits presence of heterocyclic compound and this is further proven by the possible presence of nitrogen atoms due to C-N stretching at 1091 cm^{-1}. The presence of nitrogen atom maybe derived during the preparation and exfoliation of graphene nanosheets using nitric acid [24].

INSERT FIG. 4 HERE

3.2 Thermal conductivity of nanofluids

3.2.1 Effect of temperature

Generally, the thermal conductivity of graphene nanosheet – hydrogenated oil-based nanofluid increases linearly to a certain extent with respect to temperature as shown in Fig. 7. Similar trends were also observed by other researcher [14,23,25]. The increase in thermal conductivity properties of nanofluids is attributed to the increased movement of Brownian motion and micro-convection of nanoparticles at higher temperatures [26] due to the influences of phonons, free electrons and molecular diffusion and collision [15]. At higher temperature, heat transfer is improved due to higher phonon vibrations and rapid collisions of molecules to enhance thermal conductance between suspended solid nanoparticles.

INSERT FIGURE 5 HERE

3.1.2 Comparison of experimental results and thermal conductivity models

The analysis of graphene nanosheets dispersed in hydrogenated oil-based fluids was carried out in the range of 30°C, 40°C and 50°C over particle loadings at 25 ppm, 50 ppm and

100 ppm. In this study, classical thermal conductivity models were employed to predict the accuracy of thermal conductivity data obtained from experimental methods.

Classical thermal conductivity models used are Maxwell model [27], Hamilton and Crosser (HC) model [23] and Bruggeman model [24]. These conventional thermal conductivity models incorporate several key important parameters including thermal conductivity of nanoparticle (k_p), thermal conductivity of base fluid (k_f), nanoparticle loadings (φ) and shape factor (n) of nanoparticles.

Maxwell model was developed to predict suspensions containing dilute particles at concentrations less than 1 vol% [25] where particles are assumed to be spherical intrinsically and non-interacting. Maxwell model is expressed as:

$$k_{nf} = \left[\frac{k_p + 2k_{bf} + 2(k_p - k_{bf})\varphi}{k_p + 2k_{bf} - 2(k_p - k_{bf})\varphi} \right] k_{bf} \tag{5}$$

H-C model is applied when thermal conductivity of nanoparticles exceeds thermal conductivity of base liquid by 100 times ($k_p/k_{bf} > 100$). H-C model takes into account of the shape factors of nanoparticles which was extended from the Maxwell model. The shape factor (n) is outlined as the ratio of surface area of sphere with constant volume as particle to the surface area of the particle. Shape factor are incorporated in Hamilton-Crosser (H-C) model where shape factor is defined as n = 3/ψ where ψ is known as the sphericity factor. Generally, n value for spherical nanoparticles is n = 3 which was assumed in this comparison. H-C model is as shown below:

$$k_{nf} = k_{bf}\left[1+\frac{k_p+(n-1)k_{bf}+(n-1)(k_p-k_{bf})\varphi}{k_p+(n-1)k_{bf}-(k_p-k_{bf})\varphi}\right] \quad (6)$$

Unlike Maxwell model, Bruggeman model does no possess any limitations on particle concentrations. The model is applied on binary mixtures with the assumption of particle shapes being suspended in spherical form. The effective thermal conductivity of nanofluid estimated using Bruggeman model as shown in Eq. 7.

$$\varphi\left(\frac{k_p-k_{eff}}{k_p+2k_{eff}}\right)+(1-\varphi)\left(\frac{k_p-k_{eff}}{k_p+2k_{eff}}\right)=0 \quad (7)$$

INSERT FIGURES 6, 7 AND 8 HERE

From Fig. 6 to Fig. 8, all thermal conductivity models gave similar predictions at lower nanoparticle loadings. However, the trend continues to underpredict at higher nanoparticle loadings. This is because Maxwell and Bruggeman model assumed that all particle shapes are spherical in nature [26]. Furthermore, H-C model is reduced to Maxwell model when shape factor is assumed to be $n = 3$. The shape factor was manipulated to obtain a better prediction at $n = 1$, where the prediction is similar to the experimental data at low concentration but further deviates at higher nanoparticle concentrations. Similar findings by other researchers showed that conventional static thermal conductivity models usually underpredicted the experimental data [18,27]. Gupta et al. [25] attributed this to the role of particle sizes in the distribution and network formation for heat transfer.

3.1.3 Effective thermal conductivity of graphene nanosheets

Nan et al. model [28] was used to predict the effective thermal conductivity of graphene nanosheets. The model is given by Eq. 8.

$$k_{nf} = k_{bf}\left[\frac{3+\varphi\left[2\beta_{11}(1-L_{11})+\beta_{33}(1-L_{33})\right]}{3-\varphi\left(2\beta_{11}L_{11}+\beta_{33}L_{33}\right)}\right] \tag{8}$$

where β_{11} and β_{33} is defined as

$$\beta_{11} = \frac{k_p - k_{bf}}{k_{bf} + L_{11}\left(k_p - k_{bf}\right)} \qquad \beta_{33} = \frac{k_p - k_{bf}}{k_{bf} + L_{33}\left(k_p - k_{bf}\right)} \tag{9}$$

L_{ii} is the geometrical factor in which the factors are set as $L_{11} = 0$ and $L_{33} = 1$ respectively due to the high aspect ratio of the nanoparticles.

INSERT FIGURE 9 HERE

The effective thermal conductivity of graphene nanosheets calculated by Nan et al. model is taken to be at 4.78 ± 1.6 W m^{-1} K^{-1} at 50°C. Comparison between the calculated effective thermal conductivity and intrinsic value of graphene nanosheets [12] showed a drastic drop in thermal conductivity properties. Nan et al. model takes into account the matrix additive interface contact resistance into consideration [16] which yielded lower effective thermal conductivity of nanoparticles when dispersed in hydrogenated oil-based fluid. The model also showed a drastic reduction in thermal conductivity values of nanoparticles as compared to intrinsic values of graphene nanosheets [29] . Similar findings by other researchers showed an extreme drop in the effective thermal conductivity of nanoparticles as well [14,16,26].

Surface defects found on the surface of nanoparticles contributed to the fluctuations of thermal conductivity of solid nanoparticles. Yu et al. [16] and Kole and Dey [14] explained that oxidation of graphite for the synthesise of graphene nanosheets imposed severe lattice defects on the surface of nanoparticles. Furthermore, hydrodynamic cavitation utilizes very high amount of explosive energy for dispersion and breaking down of agglomerate into smaller clusters. This large amount of energy applied during homogenization process could

lead to the straining of nanoparticle structures at micro level to form bends and kinks.

3.2 Rheological behaviour of nanofluids

3.2.1 Rheological profile

The rheological behaviour of hydrogenated oil-based fluid follows characteristics of non – Newtonian fluids. Bingham fluids behave rigidly at very low stresses but flow as viscous fluids when sufficient stress is applied. Although hydrogenated oil-based fluid follows similar to Newtonian profile as shown in Fig. 10(a), the viscosity profiles shown in Fig. 10(b) depicted a shear thinning viscosity profile. In contrast, the viscosity profile of Newtonian fluids must be constant with respect to the shear rate for Newtonian fluids.

INSERT FIGURE 10(a) AND FIGURE 10(b) HERE

Therefore, the rheological profile denoted a non-Newtonian fluid profile close to zero yield stresses with a shear thinning behaviour profile.

3.2.2 Effect of temperature and nanoparticle concentration

The rheological behaviours were investigated at temperature of 30°C, 40°C and 50°C at graphene nanosheets concentrations of 25 ppm, 50 ppm and 100 ppm.

INSERT FIGURE 11, FIGURE 12 AND FIGURE 13 HERE

From the figures shown, addition of graphene nanosheets at very low particle concentration does not alter the rheological behaviour of hydrogenated oil-based fluid. At higher shear rate, the viscosity of hydrogenated oil-based nanofluids decreased exponentially towards base fluid's viscosity regardless of nanoparticle concentration. However, the

viscosity profile at higher shear rates showed slight thickening behaviour instead. The concentration of graphene nanosheets at 100 ppm yielded the highest viscosity as compared to 25 ppm and 50 ppm concentration at all temperatures.

INSERT FIGURE 14 HERE

From Fig. 14, the addition graphene nanosheets have increased the viscosity of nanofluids by approximately 23%, 42% and 54% at 25 ppm, 50 ppm and 100 ppm concentrations respectively. Similar to other studies carried out by other researchers, viscosity of nanofluids increases with respect to nanoparticle concentration but the viscosity profile decreases at increasing shear rates [30,31]. Higher viscosities are able to keep the cuttings suspended at low shear rates in any drilling operations to avoid sagging from occurring while drilling muds are channelled out from the wellbore [18]. The increased in solid particle concentrations within liquid suspensions heightened inter-particle frictions [32] which increases the resistance of fluid to flow and subsequently increases the viscosity of nanofluids.

The behaviour of hydrogenated oil-based nanofluids possesses two different behaviours, namely shear thinning and shear thickening behaviours as shown in Fig. 13 to Fig. 15. At very low shear rates, the nanofluids exhibit shear thinning behaviour while at higher shear rate they show a slight shear thickening behaviour. Ijam et al. [33] and Kinloch et al. [34] both attributed this rheological behaviour to the percolation structure of nanoparticles suspended in the base fluid. The percolation structure formed was broken down at high level of shearing to form primary particles and subsequently increasing shear stress at increasing shear rate.

Apart from that, temperature plays a crucial role in affecting the rheological profile of

graphene nanosheets – hydrogenated oil-based nanofluid. At higher temperature, the viscosity of all fluids at various nanoparticle concentrations yielded lower viscosity values as compared to lower temperatures at similar conditions as shown in Fig. 16. The increased in temperature resulted in higher energy into the system, which subsequently decreased the interparticle and intermolecular adhesive forces of the particles [34] leading to decreased fluid viscosity. Similar results by other researchers also show viscosity of nanofluids decreasing with respect to temperature [33,35].

3.2.3 Comparison of experimental data and rheological models

In this study, Bingham model and Power Law model were used to evaluate non-Newtonian fluids. Bingham Plastic fluids exhibit "infinite" viscosity until a sufficiently high stress is applied to initiate the liquid flow. The Bingham model is given as:

$$\sigma = \sigma_0 + \mu\gamma \tag{10}$$

where σ is given as shear stress, σ_o is the limiting shear stress, μ is the liquid viscosity and γ is the shear rate. The limiting shear stress is often referred to as Bingham yield stress of the material [36]. Bingham model is suitable for the calculation of suspensions and colloidal systems that show Bingham behaviours.

Power Law model is also referred as Ostwald model. The behaviour of fluid viscosity is differentiated into shear thinning and shear thickening behaviours when subjected to increasing shear rate. The Power Law model is given as:

$$\sigma = \mu.\gamma^n \tag{11}$$

where σ is the shear stress, μ is the fluid viscosity, γ is the shear rate and n is the power law index of the material. The power law index of the material is categorized into two, namely

n < 1 for shear thinning properties and n > 1 for shear thickening properties. Furthermore, Power Law model is only applicable within the range of 10^1 to 10^4 s^{-1} [36] where shear rate greater than the specified range will lead to deviations.

INSERT FIGURE 15, FIGURE 16 AND FIGURE 17 HERE

With the exception of 50 ppm hydrogenated oil nanofluid in Fig. 16, comparisons of experimental data against rheological models have shown Bingham model to give a better fitting as compared to Power Law model at all nanoparticle concentrations and temperature. The possible explanation for this exception is the extraction of clustered nanoparticles present at each random extraction points that had caused Bingham plastic viscosity to be generally higher than other experimental data. The higher Bingham plastic viscosity value resulted in the Bingham model to deviate further than the experimental data at 50 ppm and 40°C.

From Fig. 15 to Fig.17, the experimental data is able to fit closely to the Power Law model at lower shear rate. However, the predicted shear stress by Power Law model deviates exponentially at greater shear rate. The flow behaviour index, *n*, as shown in Eq. 11 [36] is a power factor which returns higher values when numerical value of *n* is larger due to shear thickening behaviour at higher shear rates.

3.3 Hydrodynamic cavitation evaluation

Table 3 shows the calculated value of mass flow rate, Reynold's number, cavitation number and coefficient of discharge parameters.

INSERT TABLE 3 HERE

In this study, the mass flow rate (*M*) was fixed constant at 0.0195 kg s^{-1}. The maximum velocity achieved in an undisturbed flow through the orifice was 15.92 m/s. For a

single stage high pressure homogenizer, the calculated $\sqrt{Re} > 60$ for a fully turbulent flow [21] is achieved as the calculated Reynold's number value is $\sqrt{Re}$ = 78.24. Since coefficient of discharge (C_D) increases with decreasing cavitation appearance [21], the calculated C_D was calculated to be C_D = 0.3313 which denoted a fully developed turbulent flow for a high pressure homogenizer with a single orifice setup.

Using Eq. 2, the calculated cavitation number (K) is calculated at 1.025. Theoretically, cavitation will only take place when $K < 1$ where lower K values will lead to greater cavitation for bubble implosions to occur [21]. However, Rooze et al. [37]also mentioned that the critical cavitation number varies from 0.2 to 1.5 for an orifice setup. Therefore, K value does not directly reflect the quantity or quality of a cavitation process but more towards the evaluation of a probability of a cavitation appearance [21].

4. Conclusions

In summary, this study has presented several findings from the addition of graphene nanosheet particles on hydrogenated oil-based nanofluid. The findings of this paper can be divided in terms of thermal conductivity properties and rheological properties of graphene nanosheet-hydrogenated oil-based nanofluids in addition to the evaluation of the effectivity of hydrodynamic cavitation process. At very low nanoparticle loadings, thermal conductivity of nanofluid improved accordingly to nanoparticle concentrations with maximum enhancement of 14.41% for 100 ppm of graphene nanosheets at 50°C are comparable to other literature review findings. Effective thermal conductivity of graphene nanosheets calculated from

Nan et al. model were severely reduced to 4.78 ± 1.6 W $m^{-1}K^{-1}$ as compared to its intrinsic value due to possible surface defects from exfoliation and hydrodynamic cavitation process.

Rheological behaviour shows viscosity of nanofluid increases with nanoparticle concentration with shear thinning Bingham plastic behaviour at low shear rate and slight shear thickening behaviour at higher shear rate with 54% increment in viscosity at 100 ppm concentration. Finally, the evaluation of hydrodynamic cavitation process showed that cavitation had occurred even though cavitation number (K) was calculated to be $K > 1$. However, other parameters such as critical cavitation number range, coefficient of discharge (C_D) and Reynold's number (Re) had proved that cavitation carried out. This work have also presented an alternate two-steps methods as dispersion methods for nanoparticle powder into base fluids apart from the conventional ultrasonication dispersions or homogenizations.

Acknowledgement

This research is supported by Biomass Processing Research Grant and in collaboration with Platinum Green Chemicals Sdn. Bhd. The authors would also like to thank Centralized Analytical Laboratory (CAL), Universiti Teknologi PETRONAS for their kind assistance in the FTIR analysis.

References

[1] Amani M, Al-Jubouri M, Shadravan A. Comparative Study of Using Oil-Based Mud Versus Water-Based Mud in HPHT Fields. Adv Pet Explor Dev 2012;4:18–27. doi:10.3968/j.aped.1925543820120402.987.

[2] Amanullah M, Al-Arfaj MK, Al-Abdullatif Z. Preliminary test results of nano-based drilling fluids for oil and gas field application. SPE/IADC Drill Conf Proc 2011;1:112–20.

[3] Al-yasiri MS, Al-sallami WT. How the Drilling Fluids Can be Made More Efficient by Using Nanomaterials How the Drilling Fluids Can be Made More Efficient by Using Nanomaterials 2015;3:0–5. doi:10.11648/j.nano.20150303.12.

[4] Singh S, Ahmed R. Vital Role of Nanopolymers in Drilling and Stimulations Fluid Applications. Proc SPE ATCE 2010:19–22. doi:10.2118/130413-MS.

[5] Growcock FB, Patel AD, Swaco M. The Revolution in Non-Aqueous Drilling Fluids 2011.

[6] Amorin R, Dosunmu A, Amankwah RK. Enhancing the stability of local vegetable oils (esters) for high geothermal drilling applications. J Pet Gas Eng 2015;6:90–7. doi:10.5897/JPGE2015.0215.

[7] Mukherjee S, Paria S. Preparation and Stability of Nanofluids-A Review. IOSR J Mech Civ Eng 2013;9:63–9. doi:10.9790/1684-0926369.

[8] Tasawar Hayat, Arsalan Aziz TMAA. On magnetohydrodynamic three-dimensional flow of nanofluid over a convectively heated nonlinear stretching surface.pdf. Int J Heat Mass Transf 2016;100:566–72.

[9] Dharmalingam R, Sivagnanaprabhu KK, Senthil Kumar B, Thirumalai R. Nano materials and nanofluids: An innovative technology study for new paradigms for technology enhancement. Procedia Eng 2014;97:1434–41. doi:10.1016/j.proeng.2014.12.425.

[10] Choi SUS. Nanofluids: From Vision to Reality Through Research. J Heat Transfer 2009;131:33106. doi:10.1115/1.3056479.

[11] Novoselov KS, Geim AK, Morozov SV, Jiang D, Zhang Y, Dubonos S V., et al. Electric Field Effect in Atomically Thin Carbon Films. Science (80-) 2004;306:666–9. doi:10.1126/science.1102896.

[12] Pop E, Varshney V, Roy A. Thermal properties of graphene: Fundamentals and applications. Mrs Bull 2012;1273:1–28. doi:10.1557/mrs.2012.203.

[13] Balandin AA, Ghosh S, Bao W, Calizo I, Teweldebrhan D, Miao F, et al. Superior thermal conductivity of single-layer graphene. Nano Lett 2008;8:902–7. doi:10.1021/nl0731872.

[14] Kole M, Dey TK. Investigation of thermal conductivity, viscosity, and electrical conductivity of graphene based nanofluids. J Appl Phys 2013;113. doi:10.1063/1.4793581.

[15] Ahammed N, Asirvatham LG, Titus J, Bose JR, Wongwises S. Measurement of thermal conductivity of graphene-water nanofluid at below and above ambient temperatures. Int Commun Heat Mass Transf 2016;70:66–74. doi:10.1016/j.icheatmasstransfer.2015.11.002.

[16] Yu W, Xie H, Wang X, Wang X. Significant thermal conductivity enhancement for nanofluids containing graphene nanosheets. Phys Lett Sect A Gen At Solid State Phys 2011;375:1323–8. doi:10.1016/j.physleta.2011.01.040.

[17] Ma W, Yang F, Shi J, Wang F, Zhang Z, Wang S. Silicone based nanofluids containing functionalized graphene nanosheets. Colloids Surfaces A Physicochem Eng Asp 2013;431:120–6. doi:10.1016/j.colsurfa.2013.04.031.

[18] Agarwal S, Phuoc TX, Soong Y, Martello D, Gupta RK. Nanoparticle-stabilised invert emulsion drilling fluids for deep-hole drilling of oil and gas. Can J Chem Eng 2013;91:1641–9. doi:10.1002/cjce.21768.

[19] Vajjha RS, Das DK. A review and analysis on influence of temperature and concentration of nanofluids on thermophysical properties, heat transfer and pumping power. Int J Heat Mass Transf 2012;55:4063–78. doi:10.1016/j.ijheatmasstransfer.2012.03.048.

[20] Chai YH, Yusup S, Chok VS, Arpin MT, Irawan S. Investigation of thermal conductivity of multi walled carbon nanotube dispersed in hydrogenated oil based drilling fluids. Appl Therm Eng 2016;107:1019–25. doi:10.1016/j.applthermaleng.2016.07.017.

[21] Schlender M, Minke K, Spiegel B, Schuchmann HP. High-pressure double stage homogenization processes: Influences of plant setup on oil droplet size. Chem Eng Sci 2015;131:162–71. doi:10.1016/j.ces.2015.03.055.

[22] Ozonek J, Lenik K. Effect of different design features of the reactor on hydrodynamic cavitation process. Arch Mater Sci Eng 2011;52:112–7.

[23] Farbod M, Ahangarpour A, Etemad SG. Stability and thermal conductivity of water-based carbon nanotube nanofluids. Particuology 2014;22:1–7. doi:10.1016/j.partic.2014.07.005.

[24] Haddad Z, Abid C, Oztop HF, Mataoui A. A review on how the researchers prepare their nanofluids. Int J Therm Sci 2014;76:168–89. doi:10.1016/j.ijthermalsci.2013.08.010.

[25] Gupta SS, Siva M V, Krishnan S, Sreeprasad TS, Singh PK, Pradeep T, et al. Thermal conductivity enhancement of nanofluids containing graphene nanosheets. J Appl Phys 2011;110:84302. doi:10.1063/1.3650456.

[26] Hadadian M, Goharshadi EK, Youssefi A. Electrical conductivity, thermal conductivity, and rheological properties of graphene oxide-based nanofluids. J Nanoparticle Res 2014;16. doi:10.1007/s11051-014-2788-1.

[27] Yu W, Choi SUS. The role of interfacial layers in the enhanced thermal conductivity of nanofluids: A renovated Maxwell model. J Nanoparticle Res 2003;5:167–71.

doi:10.1023/A:1024438603801.

[28] Lee J-H, Lee S-H, Choi CJ, Jang SP, Choi SUS. A Review of Thermal Conductivity Data, Mechanisms and Models for Nanofluids. Int J Micro-Nano Scale Transp 2011;1:269–322. doi:10.1260/1759-3093.1.4.269.

[29] Li H, Wang L, He Y, Hu Y, Zhu J, Jiang B. Experimental investigation of thermal conductivity and viscosity of ethylene glycol based ZnO nanofluids. Appl Therm Eng 2014;88:363–8. doi:10.1016/j.applthermaleng.2014.10.071.

[30] Ding Y, Alias H, Wen D, Williams RA. Heat transfer of aqueous suspensions of carbon nanotubes (CNT nanofluids). Int J Heat Mass Transf 2006;49:240–50. doi:10.1016/j.ijheatmasstransfer.2005.07.009.

[31] Eastman JA, Choi SUS, Li S, Yu W, Thompson LJ. Anomalously increased effective thermal conductivities of ethylene glycol-based nanofluids containing copper nanoparticles. Appl Phys Lett 2001;78:718–20. doi:10.1063/1.1341218.

[32] Lu G, Duan YY, Wang XD. Surface tension, viscosity, and rheology of water-based nanofluids: a microscopic interpretation on the molecular level. J Nanoparticle Res 2014;16. doi:10.1007/s11051-014-2564-2.

[33] Ahammed N, Asirvatham LG, Wongwises S. Effect of volume concentration and temperature on viscosity and surface tension of graphene-water nanofluid for heat transfer applications. J Therm Anal Calorim 2016;123:1399–409. doi:10.1007/s10973-015-5034-x.

[34] Ijam A, Saidur R, Ganesan P, Moradi Golsheikh A. Stability, thermo-physical properties, and electrical conductivity of graphene oxide-deionized water/ethylene glycol based nanofluid. Int J Heat Mass Transf 2015;87:92–103.

doi:10.1016/j.ijheatmasstransfer.2015.02.060.

[35] Kinloch IA, Roberts SA, Windle AH. A rheological study of concentrated aqueous nanotube dispersions. Polymer (Guildf) 2002;43:7483–91. doi:10.1016/S0032-3861(02)00664-X.

[36] Ghadimi A, Saidur R, Metselaar HSC. A review of nanofluid stability properties and characterization in stationary conditions. Int J Heat Mass Transf 2011;54:4051–68. doi:10.1016/j.ijheatmasstransfer.2011.04.014.

[37] Rao A. Chapter 3:Measurement of flow and viscoelastic properties. Rheol Fluid, Semisolid, Solid Foods - Princ Appl 2013;19:461. doi:10.1007/978-1-4614-9230-6.

[38] Rooze J, André M, Van Der Gulik GJS, Fernández-Rivas D, Gardeniers JGE, Rebrov E V., et al. Hydrodynamic cavitation in micro channels with channel sizes of 100 and 750 micrometers. Microfluid Nanofluidics 2012;12:499–508. doi:10.1007/s10404-011-0891-5.

LIST OF TABLES

Hydrogenated Oil		Graphene Nanosheets	
Density (kg/m^3)	780 (at 15°C)	**Density (kg/m^3)**	874.4
Viscosity (cP)	1.5 – 2.0 (at 40°C)	**Carbon content (%)**	> 99.8%
Flash Point (°C)	90	**Oxygen (%)**	< 0.05
Vapour pressure (kPa)	< 0.1 (at 40°C)	**X-Y dimensions (µm)**	0.06 – 0.1
		Z dimensions (µm)	0.002 – 0.005
		Thermal conductance (W/m.K)	2800

Table 1: Summary of physical properties of hydrogenated oil-based drilling fluid and graphene nanosheets.

Parameters	Dimensions
Orifice diameter, $d_{orifice}$	0.00100 m
Pipe diameter, d_{pipe}	0.0186 m
Pressure drop, Δp	900,000 Pa

Table 2: Summary of key parameters for hydrodynamic cavitation

Parameters	Dimensions
Mass flow rate, *M*	0.0195 kg/s
Maximum orifice velocity, μ_{max}	15.92 m/s
Reynold's number, *Re*	6121.35
Coefficient of discharge, C_D	0.3313
Cavitation number, *K*	1.025

Table 3: Summary of calculated parameters for hydrodynamic cavitation

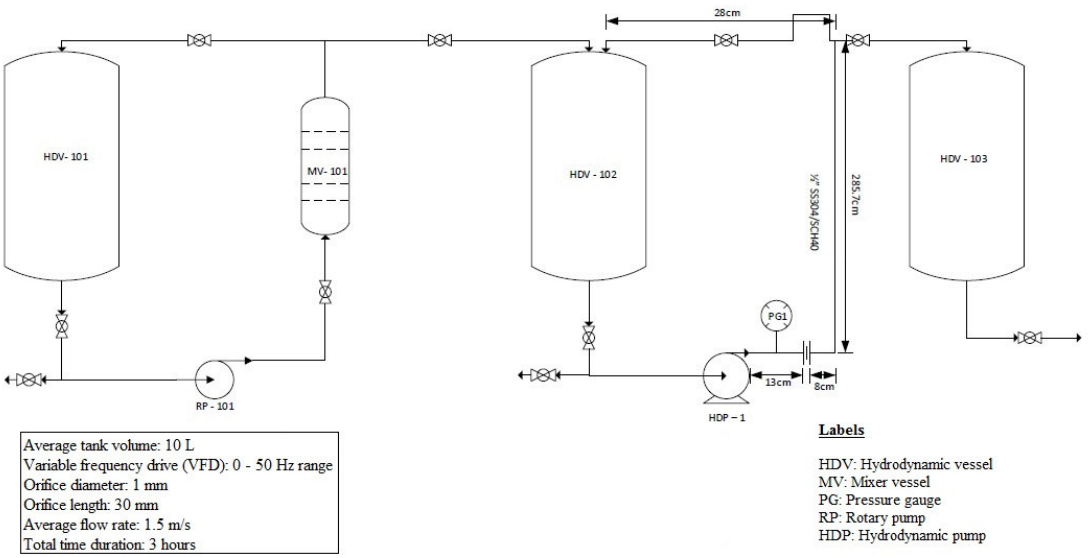

Fig. 1: Schematic diagram of hydrodynamic cavitation unit

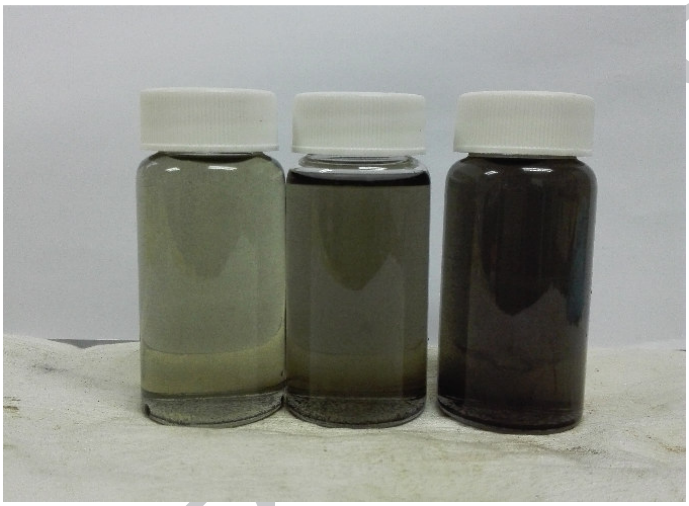

Fig. 2: Synthesized graphene nanosheet-hydrogenated oil-based nanofluids at 25 ppm (left), 50 ppm (middle) and 100 ppm (right)

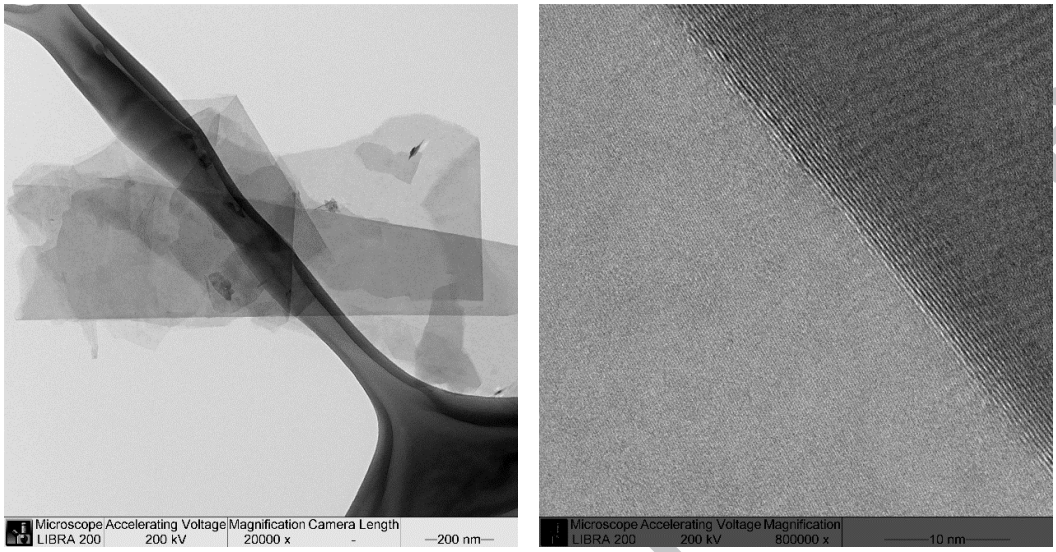

(a) (b)

Fig. 3: TEM image of graphene nanosheet at (a) 20,000x and (b) 800,000x magnification

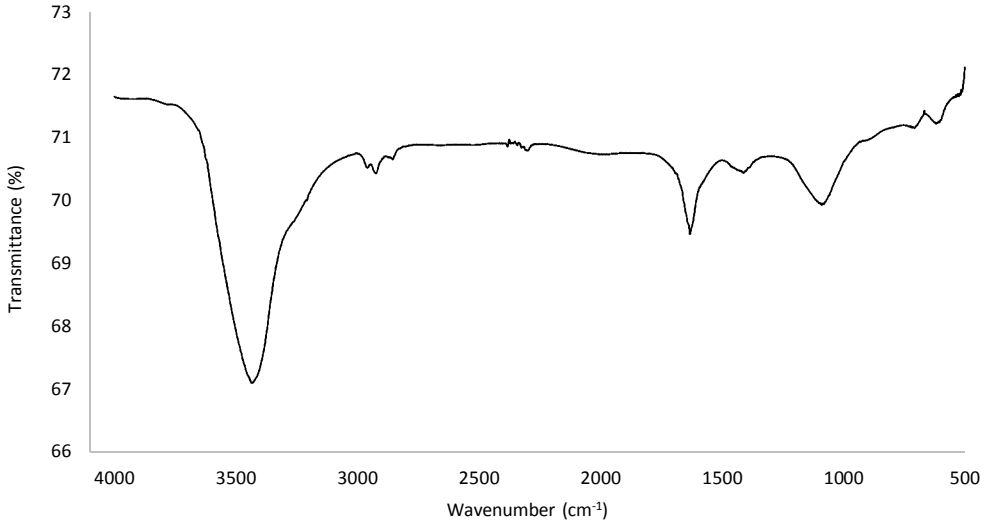

Fig. 4: FTIR spectra of graphene nanosheets

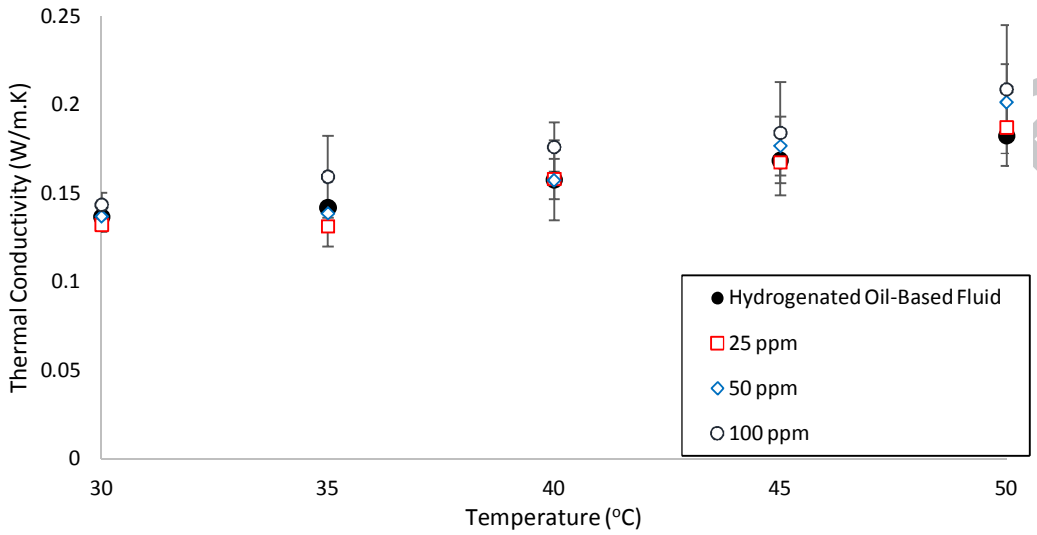

Fig. 5: Comparison of thermal conductivity of graphene nanosheets-hydrogenated oil-based nanofluids with respect to temperature and concentrations.

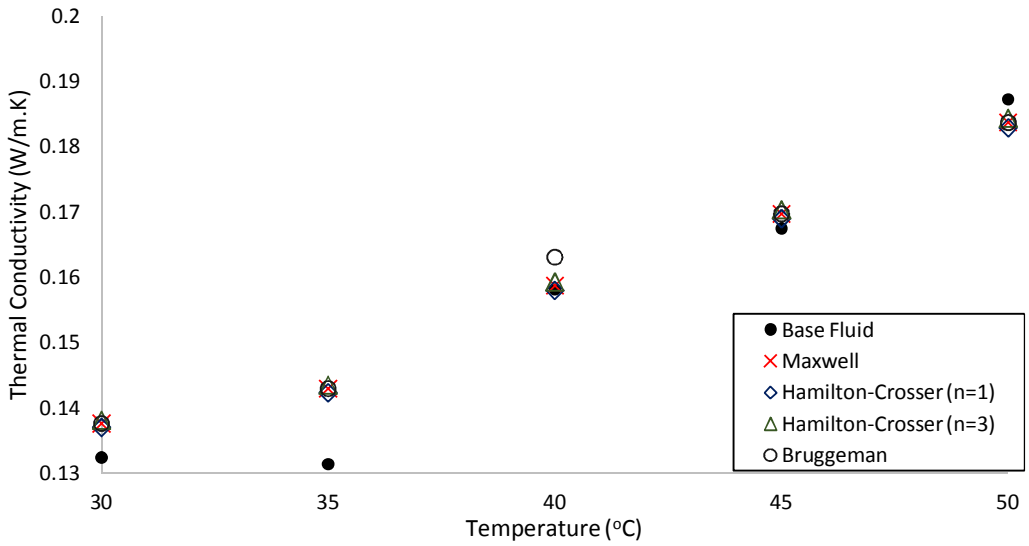

Fig. 6: Comparison between experimental data and thermal conductivity models at 25 ppm graphene nanosheet-hydrogenated oil based nanofluids

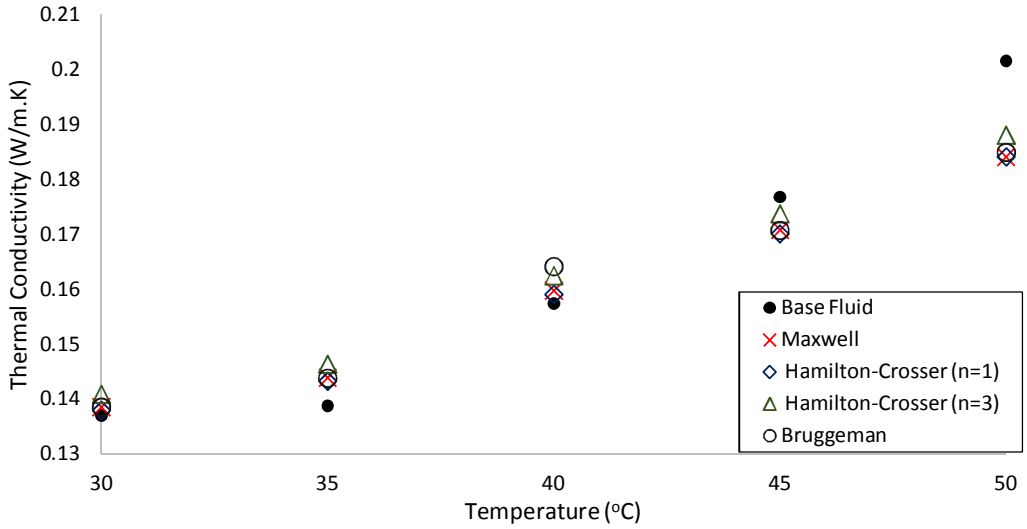

Fig. 7: Comparison between experimental data and thermal conductivity models at 50 ppm graphene nanosheet-hydrogenated oil based nanofluids

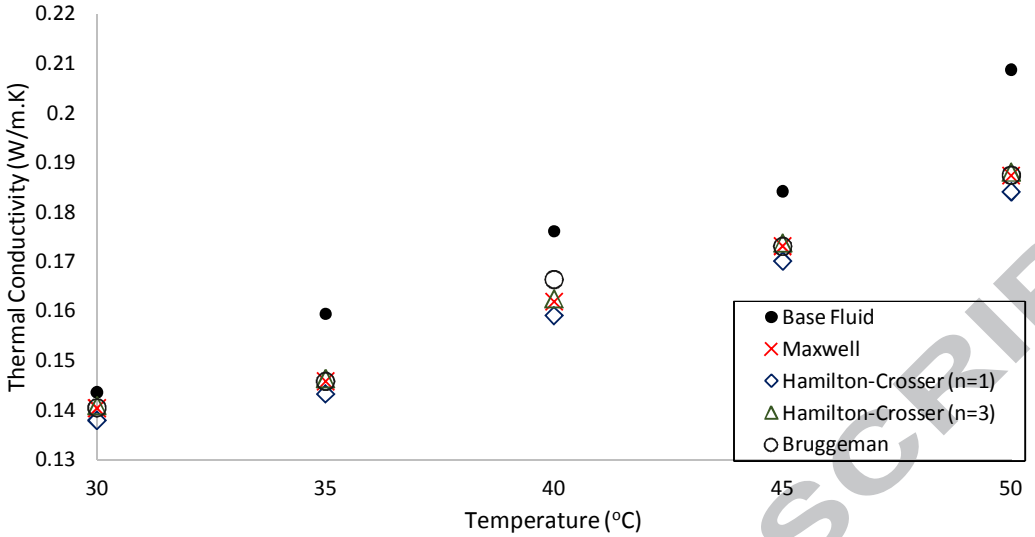

Fig. 8: Comparison between experimental data and thermal conductivity models at 100 ppm graphene nanosheet-hydrogenated oil based nanofluids

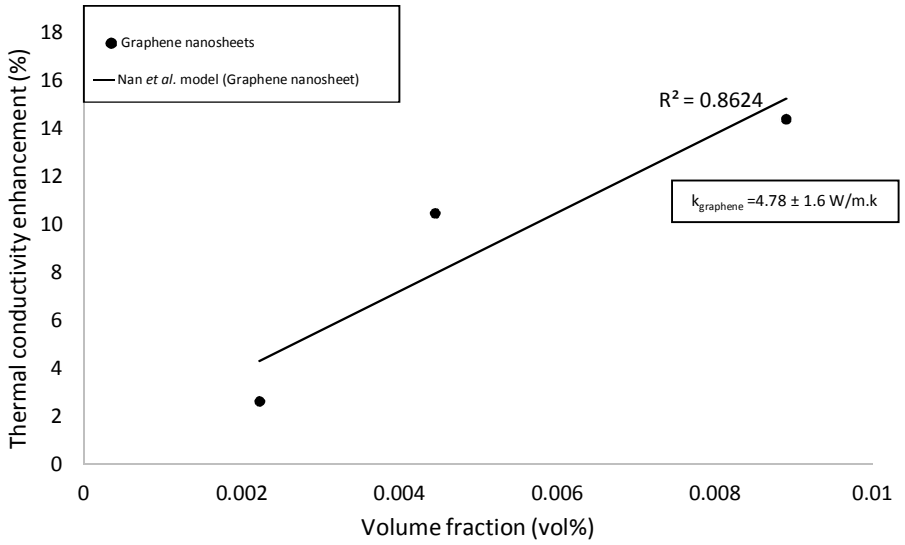

Fig. 9: Effective thermal conductivity of graphene nanosheets estimated by Nan et al. model.

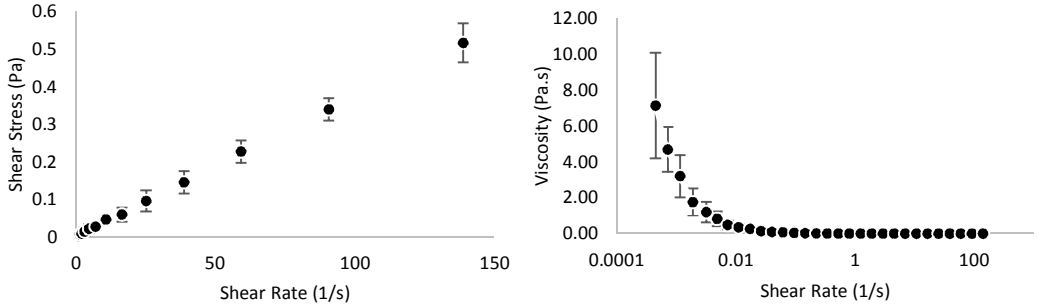

(a) (b)

Fig. 10: Graphical illustration of (a) shear stress and (b) viscosity with respect to shear rate of hydrogenated oil-based fluid at 30°C

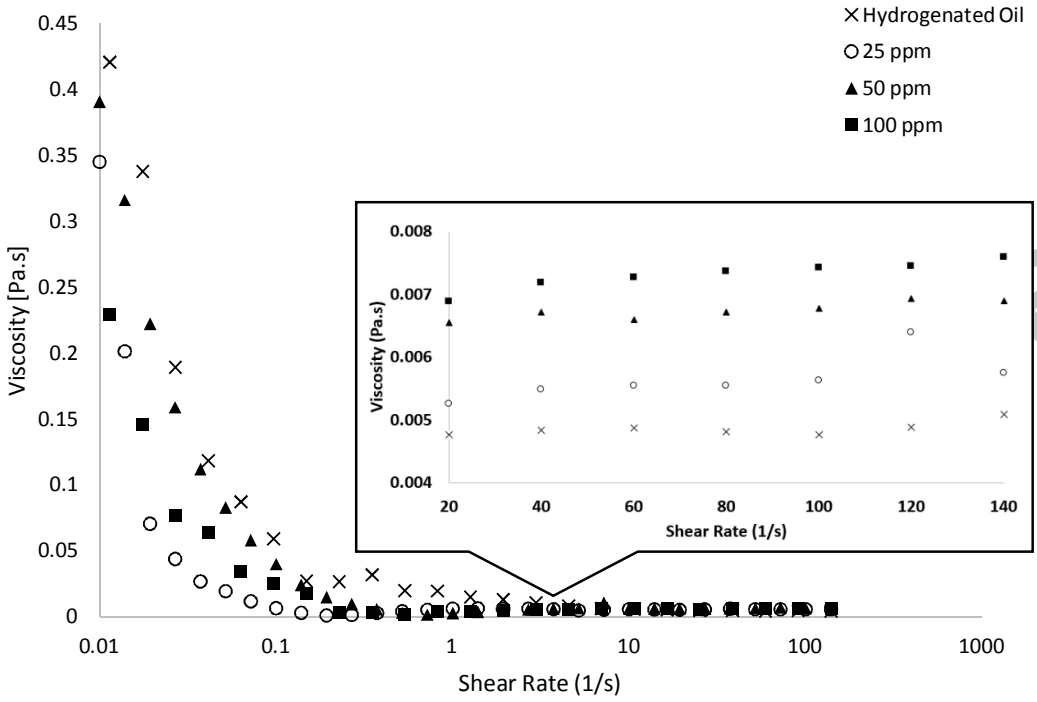

Fig. 11: Comparison between viscosities at different temperatures and increasing shear rate of graphene nanosheet-hydrogenated oil-based nanofluid at 30°C

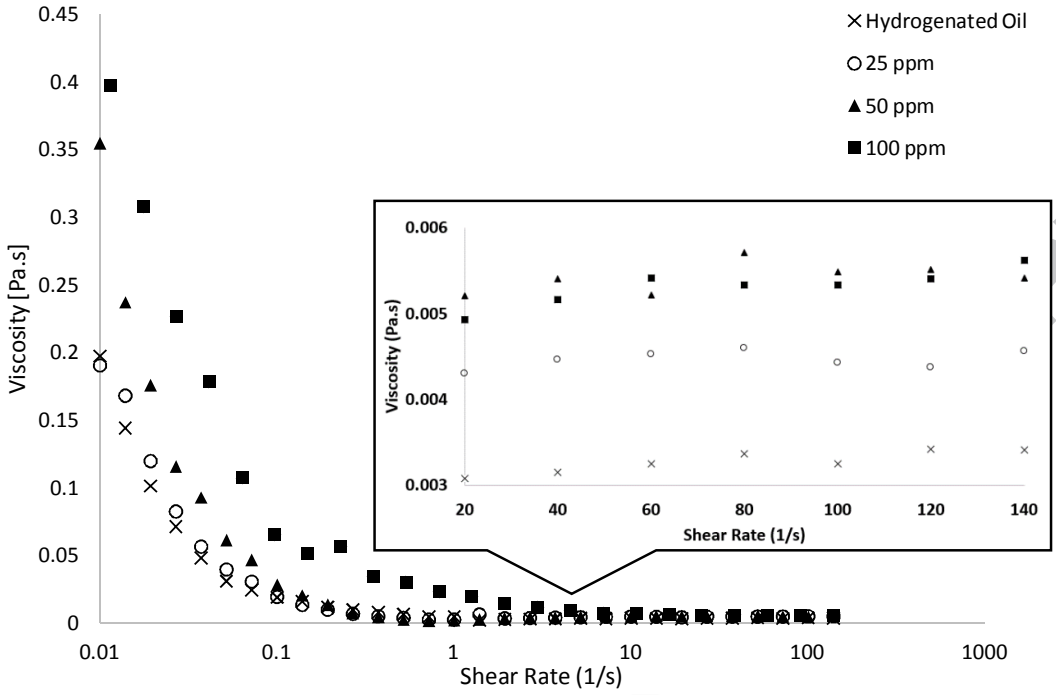

Fig. 12: Comparison between viscosities at different temperature and increasing shear rate of graphene nanosheet-hydrogenated oil-based nanofluid at 40°C

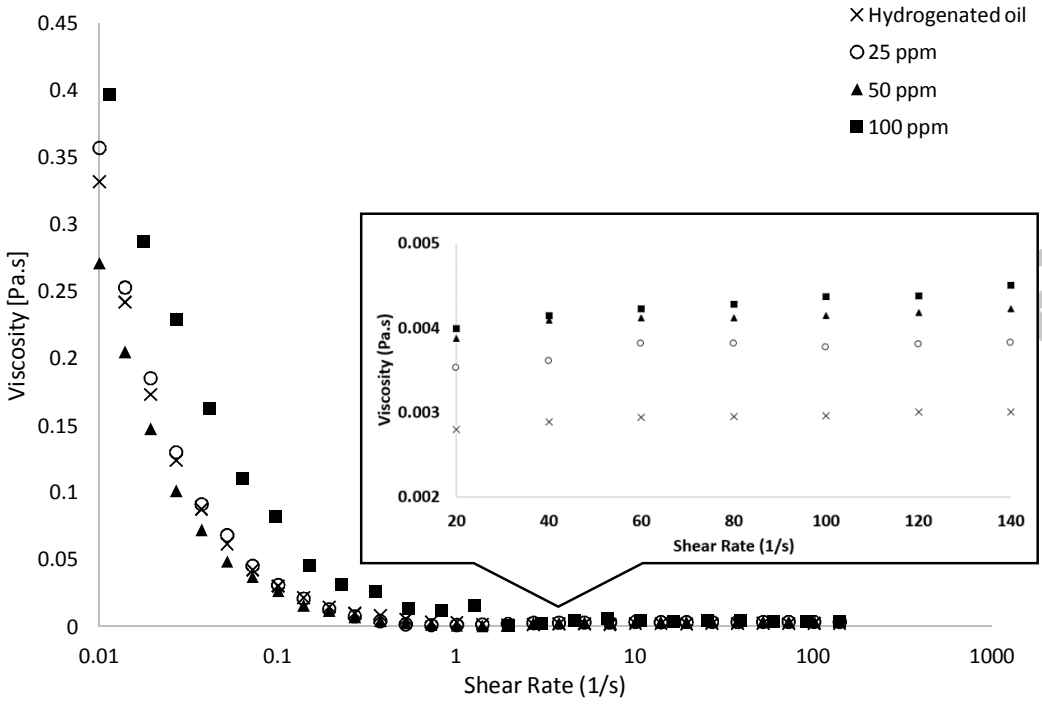

Fig. 13: Comparison between viscosities at different temperature and increasing shear rate of graphene nanosheet-hydrogenated oil-based nanofluid at 50°C

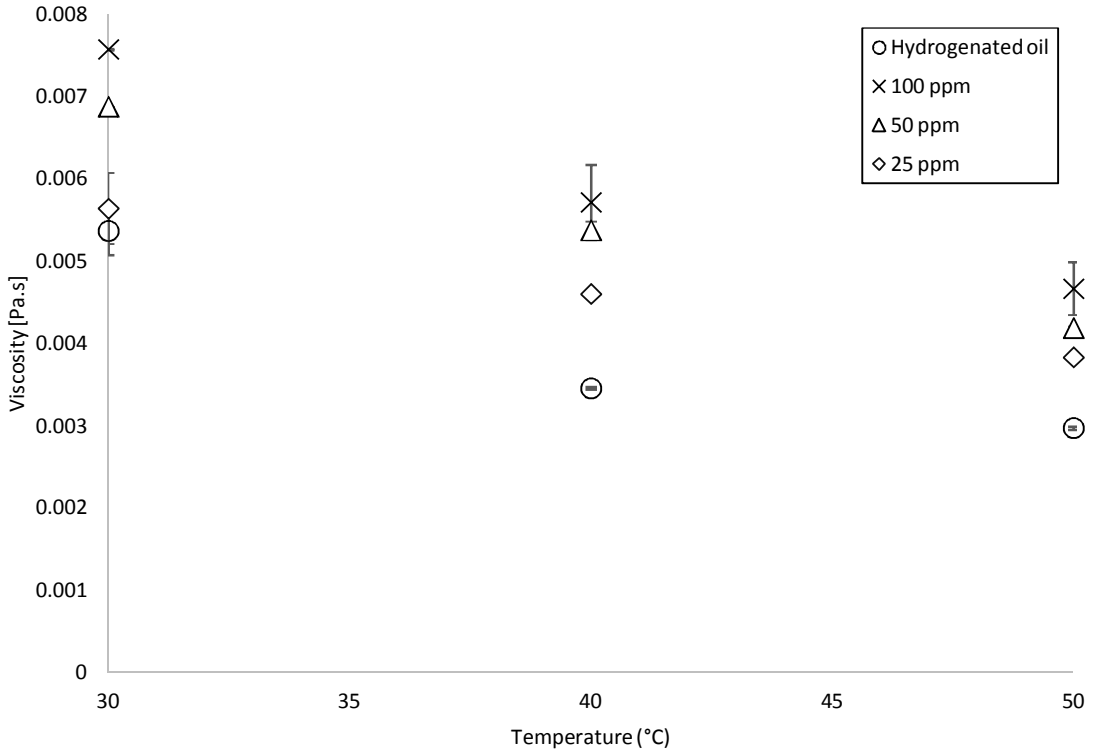

Fig. 14: Viscosity comparison of graphene nanosheet-hydrogenated oil-based nanofluids with respect to nanoparticle concentration and temperature.

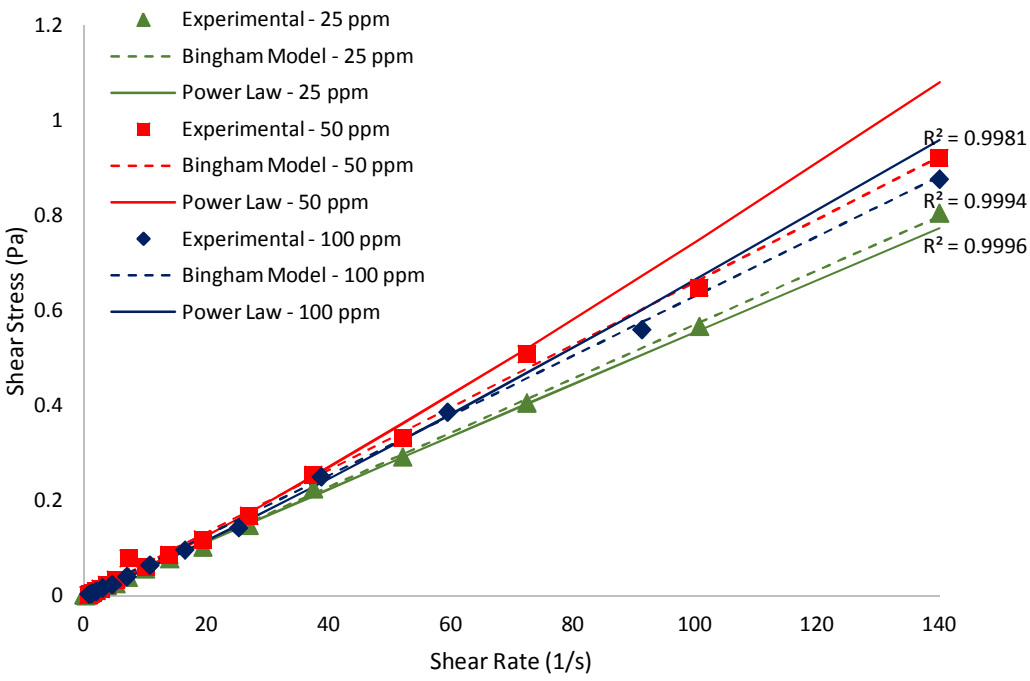

Fig. 15: Comparison between experimental data and rheological models of graphene nanosheet-hydrogenated oil-based nanofluid at 30°C

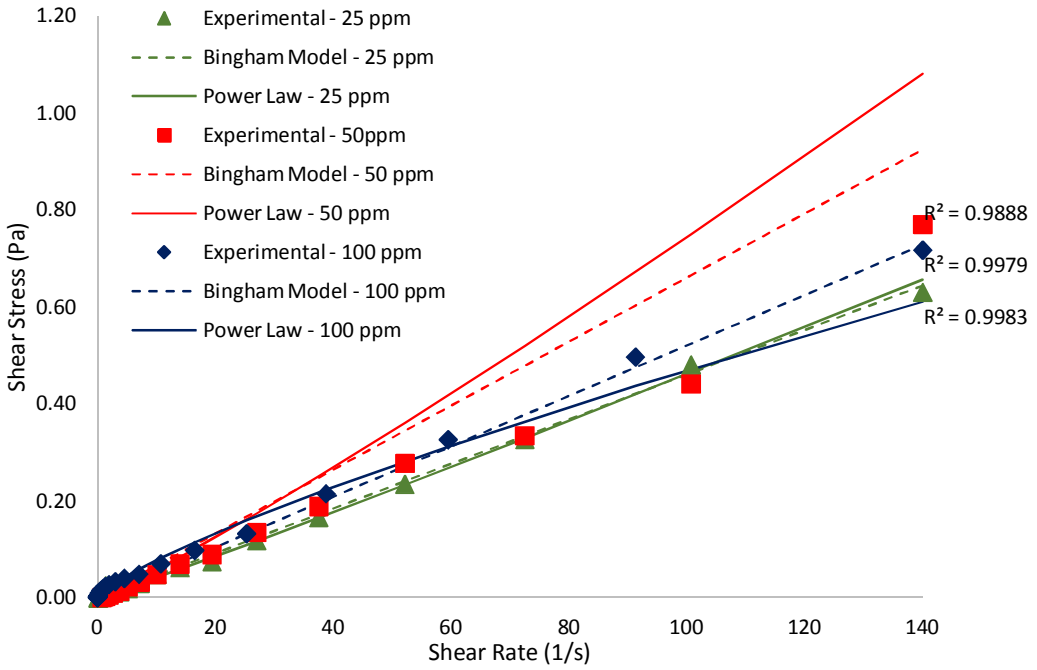

Fig. 16: Comparison between experimental data and rheological models of graphene nanosheet-hydrogenated oil-based nanofluid at 40°C

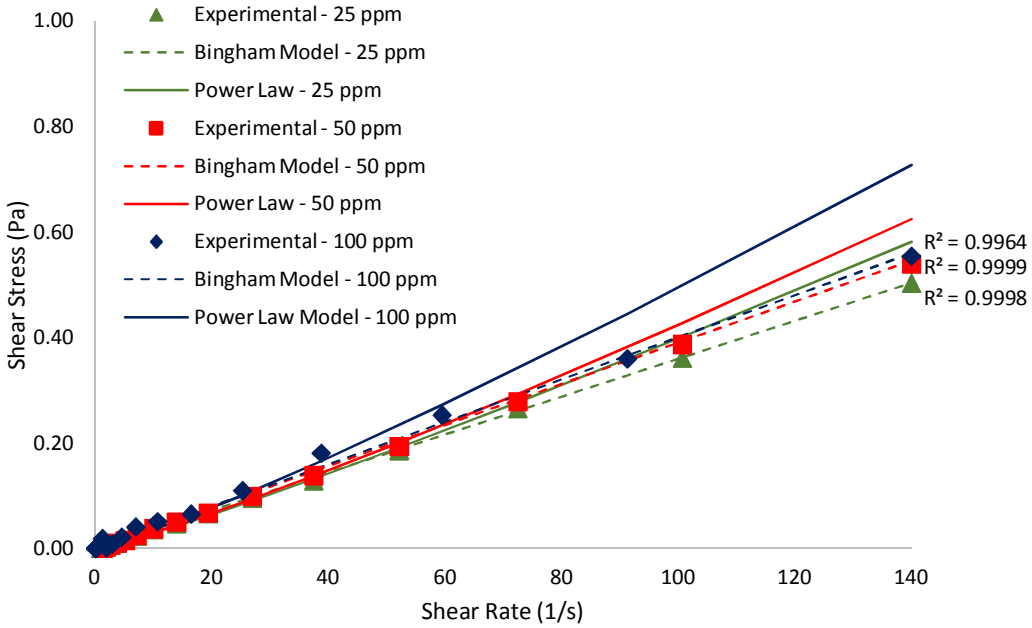

Fig. 17: Comparison between experimental data and rheological models of graphene nanosheet-hydrogenated oil-based nanofluid at 50°C

Highlights

- Combination of hydrodynamic and acoustic cavitation for nanoparticle dispersion.
- Dispersion of graphene nanosheets at 25 ppm, 50 ppm and 100 ppm.
- Thermal conductivity and rheological properties of nanofluid are investigated.
- Brief evaluation of hydrodynamic cavitation process carried out in this study.